# Alpha-radioimmunotherapy as a novel therapeutic option against metastasis of gastric cancer

# （転移性胃がんに対する新規 α 線放射免疫療法）

千葉大学大学院医学薬学府

先端医学薬学専攻

（主任：鎌田正教授）

李　惠子

# Contents


1 Introduction
- 1.1 Gastric cancer
  - 1.1.1 Peritoneal metastasis of gastric cancer
  - 1.1.2 HER2 expression in gastric cancer
- 1.2 Radioimmunotherapy
  - 1.2.1 Alpha-particle
  - 1.2.2 Astatine-211

2 Aims

3 Materials and Methods
- 3.1 Cells
- 3.2 Antibody and regents
- 3.3 Production of astatine-211
- 3.4 Immunoconjugate and astatine-211 labeling
- 3.5 Radiochemical purity
- 3.6 Serum stability
- 3.7 Western blot assay
- 3.8 Cell binding and inhibition assay
- 3.9 *In vitro* cytotoxicity
- 3.10 Animal experiments
  - 3.10.1 Xenograft mouse model
  - 3.10.2 Biodistribution
  - 3.10.3 Radioimmunotherapy in s.c. mice
  - 3.10.4 Radioimmunotherapy in PMGC mice
- 3.11 Immunofluorescence and Immunohistrical staining
- 3.12 Statistical analysis

4 Results

4.1 $^{211}$At-labeled trastuzumab specifically targets and ablates HER2-positive human cancer cells.
4.2 $^{211}$At-trastuzumab shows antitumor activity against s.c. xenografts of HER2-positive GC cells.
4.3 Establishment of a xenograft mouse model of PMGC.
4.4 More efficient delivery of $^{211}$At-trastuzumab to PMGC with i.p. rather than i.v. injection.
4.5 Locoregionally administered $^{211}$At-trastuzumab efficiently treats HER2-positive PMGC in a mouse model.
4.6 Excretion and adverse effect of i.p. injected $^{211}$At-trastuzumab in PMGC mouse model.
4.7 DNA damage is induced in tumor cells by $^{211}$At-trastuzumab.

5 Discussion

6 Conclution

7 Acknowledgement

8 Abbreviations

9 References

# 1． Introduction

## 1.1 Gastric cancer

Gastric cancer (GC) is one of the main causes of cancer-related death worldwide.(1) About 952,000 new cases diagnosed in 2012. GG is more common in Asia than other area; the Republic of Korea comes to the highest rate, followed by Mongolia and Japan. It is more common in older adults than the young, and men tend to be twice higher than women. The bacterium Helicobacter pylori, tobacco use and consumption of alcoholic drinks and processed meat are raised as the cause of GC. GC is curable at early stage, however, because of the asymptomatic most patients are diagnosed at late stage and they already have metastasis at the time of diagnosis. Currently, the standard therapeutic options for GC are surgery, radiotherapy, chemotherapy, targeted therapy and Immunotherapy.

### 1.1.1 Peritoneal metastasis of gastric cancer

Metastatic dissemination of GC to the peritoneal cavity frequently occurs during the progression of this disease and is the main form of GC relapse after surgical resection. The prognosis for peritoneal metastasis of gastric cancer (PMGC) or its associated clinical condition (peritoneal carcinomatosis) is extremely poor and, because no effective therapeutics have been established, the mean survival time is only 4 months.(2)

### 1.1.2 HER2 expression in GC

Recent advances in the molecular dissection of GC have helped to identify reliable predictive biomarkers, allowing introduction of molecular targeted drug therapy. Approximately 20% of GCs are HER2-positive.(3,4) Therefore, HER2 is an attractive target for GC. Trastuzumab, an anti-HER2 mAb, has been used previously as a targeted therapy for HER2-positive GC and yields excellent treatment outcomes.(4) However, its therapeutic efficacy is still limited for patients with PMGC. Novel antitumor strategies are thus still required to improve the clinical outcomes

for GC patients, particularly those with PMGC.

### 1.2 Radioimmunotherapy

Radioimmunotherapy is a targeted radioisotope treatment method that uses an antibody as a carrier of therapeutic radioisotopes and has considerable advantages when used against micrometastatic or disseminated tumors.(5–8) The selective targeting of radioisotopes to the tumor using a radiolabeled cancer-specific antibody enables the delivery of a high dose of radiation directly to cancer cells while minimizing the exposure of normal cells.

#### 1.2.1 Alpha-particle

Among the radioisotopes used for RIT, alpha-particle emitting radioisotope (α-RI) is of particular interest because it emits highly cytotoxic α-particles. Alpha-particles emitted through the decay deposit a huge amount of energy (approximately 100 keV/lm) within a few cell diameters (a 55–80-lm path length in soft tissue) to induce irreparable DNA damage but sparing the surrounding normal tissue.(9,10) A single a-particle atom can kill a target cell, making it one of the most potent cell-killing agents available.(11,12) Alpha-RI is therefore particularly suited to the targeted killing of disseminated or micrometastatic solid tumors that are usually resistant to the low energy radiation used routinely in clinical settings, such as X-rays and b-particles.

#### 1.2.2 Astatine-211 ($^{211}$At)

Astatine-211 ($^{211}$At) is one of the attractive α-RI, which is produced via $^{209}$Bi(α, 2n)$^{211}$At reaction using cyclotron. $^{211}$At is a radiohalogen and does not have any stable isotopes. The half-life is 7.2 h, which tends to be short among therapeutic radioisotopes. $^{211}$At has two decay branches and both associated with α-emission. Since K X-rays is emitted by electron capture decay to $^{211}$Po, it enable us to get SPECT imaging to track and quantify $^{211}$At activity and distribution. The mean linear energy transfer of $^{211}$At is 97 keV/μm and the average energy is 6.79 MeV. The tissue range of $^{211}$At

is 55-70 μm, which is about few cell length.

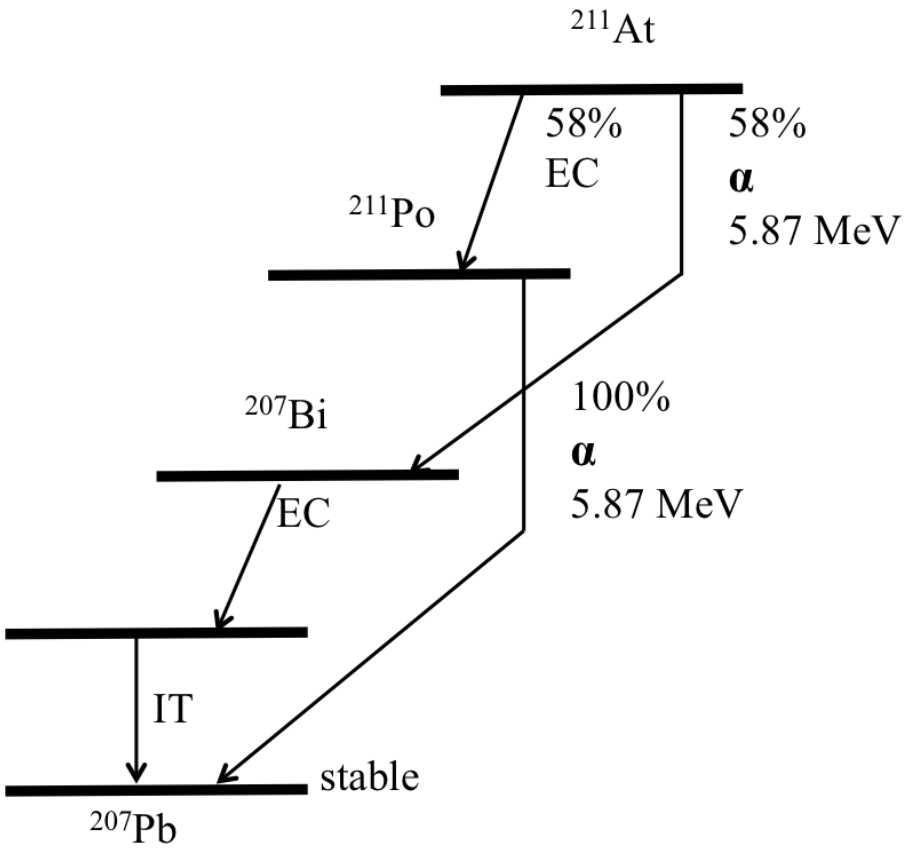


Fig.1 Scheme of decay branches of $^{211}$At

## ２． Aims

The aim of this study is to investigate the therapeutic efficacy of α-RIT using $^{211}$At-trastuzumab in preclinical mouse models of HER2-positive PMGC.

# ３． Materials and Methods

## 3.1 Cells

The human GC cell line NCI-N87 (N87) and two human breast cancer cell lines (SKBR3 and AU565) were purchased from ATCC (Manassas, VA, USA). The human GC cell line MKN45 was purchased from the Japanese Collection of Research Bioresources Cell Bank (Ibaraki, Japan). The human GC cell line MKN7 was purchased from RIKEN Cell Bank (Tsukuba, Japan). N87/Luc cells were established by the introduction of RediFect Red-FLuc-Puromycin lentiviral particles in accordance with the manufacturer's instructions (PerkinElmer, Waltham, MA, USA).

## 3.2 Antibody and reagents

Trastuzumab, an anti-HER2 mAb, was purchased from Chugai Pharmaceutical (Tokyo, Japan). N-Succinimidyl-3-(trimethylstannyl)benzoate was purchased from Santa Cruz Biotechnology (Dallas, TX,USA). N-Chlorosuccinimide (NCS) was purchased from Tokyo Chemical Industry (Tokyo, Japan).

## 3.3 Production of $^{211}$At

$^{211}$At was produced via the $^{209}$Bi(α, 2n)$^{211}$At reaction using vertical beam irradiation system of AVF-960 cyclotron (Sumitomo Heavy Industries, Tokyo, Japan) at National Institute of Radiological Sciences (Chiba, Japan).(13) After irradiation, $^{211}$At was collected in chloroform with dry distillation and the chloroform was evaporated by heating at 90˚C under high-purity nitrogen ($N_2$) gas.

## 3.4 Immunoconjugation and astatine-211 labeling

The $^{211}$At labeling of trastuzumab was carried out in accordance with a previously described direct astatination procedure.(14) Briefly, 2 μl of m-MeATE stock chloroform solution was taken and let the chloroform to be evaporated using $N_2$ gas. m-MeATE was redissolved with 10μl of

dimethyl sulfoxide. Trastuzumab was dissolved with 0.2 M sodium carbonate buffrt (pH 8.5) at a concentration of 3-5 mg/ml. m-MeATE was added to 1 mg of trastuzumab at the ratio 2 µl/mg and let the reaction continue for 30 min during gentle agitation. The immunoconjugate was then isolated using size exclusion chromatography with Sephadex 50 spin column (GE Healthcare) in PBS (730 g, 2 min, room temperature) and kept 4˚C. Before the radiolabeling, trastuzumab solution was diluted to the concentration 2 mg/ml and adjusted to pH 5.5 by adding 3% of citric acid. NCS (10 µl, 0.04 mg/ml in methanol with 1% acetic acid) were added to about 37-74 MBq of dry $Na^{211}At$ to prepare $^{211}At$ for labeling and reacted with 100 µl of m-MeATE-trastuzumab immnoconjugates (2 mg/ml) for 1 min with voltexing. 3 µl of NCS (2 mg/ml) were added and mixed for 1 min. At the end of the reaction, 5 µl of sodium ascorbate (50 mg/ml) were added to stop the reaction. $^{211}At$-trastuzumab was isolated using Sephadex 50 spin column with PBS and verified by high performance liquid chromatography. The activities of $^{211}At$-trastuzumab pre/post-isolation were measured using a dose calibrator (Capintec, Ramsey, NJ, USA) and the labeling yield was calculated by dividing the post-isolation activity by the pre-isolation activity.

### 3.5 Radiochemical Purity

The radiochemical purity (RCP) of $^{211}At$-trastuzumab was determined by methanol precipitation. $^{211}At$-trastuzumab (100-200 kBq) were taken from the sample and added to 200 µl of 1% bovine serum albumin in PBS (1%BSA/PBS) in 1.5 ml tube. 500 µl of cold methanol were added and kept in ice for 5 min to let the protein precipitated. The tube was centrifuged (3000 rpm, 3 min, 4˚C) and the supernatant was removed, the protein bound $^{211}At$ was remained in the pellet. The radioactivity of the tube before the pelleting and the pellet was measured using γ-counter (Aloka, Tokyo, Japan) with energy window 65-95 keV. The radioactivity of the pellet was measured. The radiochemical purity was calculated by dividing the radioactivity of the pellet by the applied radioactivity.

### 3.6 Serum Stability

The serum stability was evaluated in duplicate by measuring the RPC of $^{211}$At-trastuzumab after 1, 3, 15, 24 h incubation with murine serum. $^{211}$At-trastuzumab (10-12 MBq) was added to fresh prepared murine serum and incubated at 37˚C. At each time point, methanol precipitation was performed in triplicate.

### 3.7 Western blot assay

Western blot assay carried out as described previously.(8) Briefly, cell lysates was prepared in loading buffer (Cell Signaling TECHNOLOGY, Tokyo, Japan). Ten μg of cell lysates were loaded into SDS-PAGE gel (BioRad, Hercules, Tokyo) and run using an electrophoresis system. The proteins were transferred onto immunoblot membranes and incubated with primary antibodies, HER2/ErbB2 Rabbit Antibody#2242 (Cell Signaling TECHNOLOGY) or anti-α-Tublin Mouse mAb (DM1A) (MERCK MILLIPORE, Tokyo, Japan), for 1 h at room temperature followed with incubation with second antibodies, anti-Rabbit IgG HRP-linked Antibody #7074 and anti-Mouse IgG HRP-linked Antibody #7076 (Cell signaling TECHNOLOGY), as same condition. The band intensities were detected by chemiluminescence and quantified using Gene Gnome System (GGNOME-5) and Gene Sys software (SYNGENE, Cambridge, UK).

### 3.8 Cell binding and Inhibition assay

$^{211}$At-trastuzumab (approximately 25,000 cpm) was incubated with increasing concentration of either N87 or MKN45 cell suspension (1-50 x $10^5$ cells/ml in 1%BSA/PBS) in 2 ml tube on ice for 1 h. For inhibition assay, 100-fold trastuzumab was added to the cells 5 min before incubating with $^{211}$At-trastuzumab. During the incubation, the mixture in the tube was stirred with voltex every 15 min. After 1 h incubation, the tube was centrifuged (1,200 rpm, 5 min, 4˚C) and the unbound $^{211}$At-trastuzumab in the supernatant was removed. The cells were washed twice with PBS and

collected in polypropylene tube. The cell bound radioactivity was measured using a γ counter and the cell bound ratio was calculated by dividing the cell bound radioactivity by applied radioactivity.

### 3.9 In vitro cytotoxicity.

MKN45, N87, SKBR3, MKN7, and AU565 cells (2–20x$10^3$/well) were seeded into 96-well plates the day before the experiment. After the medium was removed, culture medium (100 μl) containing either PBS, trastuzumab, non-carrier $^{211}$At, or $^{211}$At-trastuzumab was applied to the cells, followed by incubation at 37°C for 24 h. The protein doses of trastuzumab and $^{211}$At-trastuzumab were adjusted to the same amount (0.0034–0.0244 μg) by the addition of intact antibody. After the incubation, the medium was removed and the cells were washed once with PBS. Fresh medium (100 μl) was then added to each well and the cells were further incubated in a humidified atmosphere containing 5% $CO_2$ at 37°C for 7 days. Cells were fixed with 4% formalin and stained with 0.05% crystal violet. The cell cytotoxicity was quantified by determining the color density of each well using Image Quant LAS4000 and Image Quant TL (GE Healthcare).

### 3.10 Animal experiments.

All animal experiments were approved by the Animal Care and Use Committee of the National Institute of Radiological Sciences at the National Institutes for Quantum and Radiological Science and Technology (Chiba, Japan) and were undertaken in compliance with the institutional guidelines regarding animal care and handling.

#### 3.10.1 Xenograft mouse model

Two types of xenograft mouse models were established for in vivo experiments. Subcutaneous gastric cancer xenograft mouse models were established by injecting N87 (8.5 x $10^6$) cells in the gluteal region subcutaneously to 5 w old BALB/cSIc-nu/nu female mice (Japan SLC, Shizuoka, Japan) 2 w before the experiment. The PMGC mouse models

were established by i.p. injecting luciferase-transfected N87/Luc cells (3 x $10^5$) into 5-week-old B17/Icr-scid/scidJcl (homo) female mice (CLEA Japan, Tokyo, Japan) 1 week before the experiment.

### 3.10.2 Biodistribution

The biodistribution of $^{211}$At-trastuzumab was determined using both s.c. and PMGC xenograft mouse models. $^{211}$At-trastuzumab was injected into the tail vein (s.c. xenograft model) or the peritoneal cavity (both xenograft models). Between four and six mice were killed at 1, 3, 6, 12, and 24 h post-injection. Tumor, whole blood, and major tissues were then sampled. All samples were weighed and the activity of $^{211}$At was measured using a c counter (Aloka, Tokyo, Japan). The %ID/g was then calculated. The $^{211}$At activity levels were measured in both the feces and urine of the PMGC model mice up to 24 h after the i.p. injection of $^{211}$At-trastuzumab and the %ID was thereby calculated.

### 3.10.3 Radioimmunotherapy in s.c. mice

RIT was performed to the mice 2 w after cell implantation. Mice were divided into 4 groups and their average tumor volume was 80.7 ± 7.7 $mm^3$. Mice received single injection of PBS, trastuzumab, 0.1 or 0.5 MBq of $^{211}$At-trastuzumab from the tail vein. All protein doses were adjusted to the same amount by adding the intact antibody. The tumor size and body weight were measured twice a week and the number of white blood cell was counted at fixed intervals. The tumor volume was calculated as length x width x height x 0.5. When the tumor volume reached 1,200 $mm^3$, the mice were euthanized. The relative tumor volume was calculated by dividing the tumor volume on the day by the volume at day 0.

### 3.10.4 Radioimmunotherapy in PMGC mice.

These PMGC model mice then underwent RIT at 1 week after cell inoculation. Mice received a single i.p. injection of PBS, trastuzumab,

non-carrier $^{211}$At (1 MBq), or $^{211}$At-trastuzumab (0.1 or 1 MBq). All protein doses were adjusted to the same amount (3.78 μg) by the addition of intact antibody except for non-carrier $^{211}$At. Tumor growth in the PMGC mice was monitored every week using an in vivo bioluminescence imaging Fusion system (Vilber Lourmat, Marne-la-Val_ee, France). Bioluminescence from PMGC was captured for 10 s at 10 min after the injection of luciferin (10 mg/mL in PBS, 300 μL/mouse). The total bioluminescence intensity in the abdominal region was quantified using Bio-1D software (Vilber Lourmat). The relative tumor intensity was calculated by dividing the tumor luminescence intensity on the day by the level at day 0. Bodyweights and white blood cell counts were determined at fixed intervals.

Blood biochemistry on glutamic oxaloacetic transaminase, glutamic pyruvate transaminase, blood urea nitrogen, and creatinine of mice injected with $^{211}$At-trastuzumab (1 MBq) was carried out using DRI-CHEM (Fujifilm, Tokyo, Japan) on the day before injection and at 1, 7, and 14 days post-injection. The mice were euthanized when the tumor luciferase intensity in the abdominal region reached 1.5 x $10^7$ photons.

### 3.11 Immunofluorescence and Immunohistochemical staining

Cells were fixed with 4% paraformaldehyde and permeabilised with 1% Triton X-100 (Sigma-Aldeich, Japan) twice for 10 min each time. Both primary and secondary antibodies mouse anti-γH2AX antibody (MERCK MILLIPORE) and anti-mouse IgG-FITC (MERCK MILLIPORE) were diluted with 4% BSA/PBS. Cells were incubated with primary antibody for 1 h at 37˚C followed washing with PBS and 1 h incubation with secondary antibody. Vectashild containing DAPI (Vector lab, CA, USA) was added to stain the DNA and covered with cover glass.

PMGC samples were either fixed with 10% buffered formalin and embedded in paraffin or filled with OTC compound after dissected from mouse and sectioned at 4 μm and 8 μm thickness, respectably. HER2 expression in PMGC was conformed by HER2 immunohistchemical

staining using Histofine® HER2 kit (Nichirei Biosciences, Tokyo, Japan) following the manufacture's instructions. Immunofluorescence staining of γH2AX in frozen section of PMGC was performed by fixing frozen section with 70% ethanol, blocking, incubated with primary antibody (mouse anti-γH2AX) for 2 h and secondary antibody (anti-mouse IgG-FITC) for another h, finally slide was mounted with Vectachield mounting medium.
Microscopic images were captured with Axio ImagerA2 microscope with microscope camera AxioCam 506 Color (Zeiss, Germany) using 100x and 40x objective for cell sample and PMGC sample, respectively.

**3.12 Statistical analyses.**

Statistical analyses were carried out with JMP version 9 software (SAS Institute Japan, Tokyo, Japan) and Statcel 3 software (OMS, Tokorozawa, Japan). Tumor volume data were analyzed using two-way repeated measures ANOVA. The survival data were analyzed with the Kaplan–Meier method. Other data were analyzed by ANOVA followed by the Tukey–Kramer post hoc test. A P-value of $<0.05$ was considered significant.

# 4. Results

## 4.1 $^{211}$At-labeled trastuzumab specifically targets and ablates HER2-positive human cancer cells.

The labeling yield of $^{211}$At-trastuzumab was 40.2 ± 6.9% and its radiochemical purity was consistently greater than 95% (Fig. 4.1). More than 88% of the $^{211}$At-trastuzumab yield was stable at 24 h after incubation with mouse serum (Fig. 4.2). We determined HER2 expression in three human GC cell lines (MKN45, N87, and MKN7), in conjunction with two human HER2-overexpressing breast cancer cell lines (SKBR3 and AU565).(8,15) The N87, SKBR3, and AU565 cells showed considerably higher HER2 expression levels relative to MKN45 cells, in which HER2 expression was very low. Expression of HER2 was found to be approximately 25-, 27-, and 24-fold higher in N87, SKBR3, and AU565 cells, respectively, than in MKN45 cells (Fig. 4.3). In addition, MKN7 cells expressed an approximately 6-fold higher HER2 level than MKN45 cells. Accordingly, we considered N87 cells to be HER2-positive GC cells and MKN45 cells to be HER2-negative GC cells. We next determined the cell binding of $^{211}$At-trastuzumab to N87 and MKN45 cells. The cell binding ratios of $^{211}$At-trastuzumab to N87 cells were much higher than those to MKN45 cells (Fig. 4.4). Moreover, the addition of a 100-fold excess of unlabeled trastuzumab markedly decreased the cell binding ratio of $^{211}$At-trastuzumab to N87 cells, suggesting that this binding was specific (Fig. 4.4).

We next evaluated the in vitro cytotoxicity of $^{211}$At-trastuzumab in MKN45, N87, SKBR3, MKN7, and AU565 cells by measuring cell viability after 24 h of exposure (Fig. 4.5). Survival was unaffected in all cases by treatment with PBS, trastuzumab, and free $^{211}$At. In contrast, a 0.37- or 1.85-kBq dose of $^{211}$At-trastuzumab effectively killed the N87, SKBR3, and AU565 cell populations and reduced the viability of MKN7 cells (Fig. 4.5). MKN45 cells were unaffected by 0.37 kBq $^{211}$At-trastuzumab and only marginally affected by 1.85 kBq $^{211}$At-trastuzumab (Fig. 4.5). Quantitative cell

viability data revealed that $^{211}$At-trastuzumab significantly reduced with the PBS and unlabeled trastuzumab controls ($P < 0.05$; Fig. 4.6).

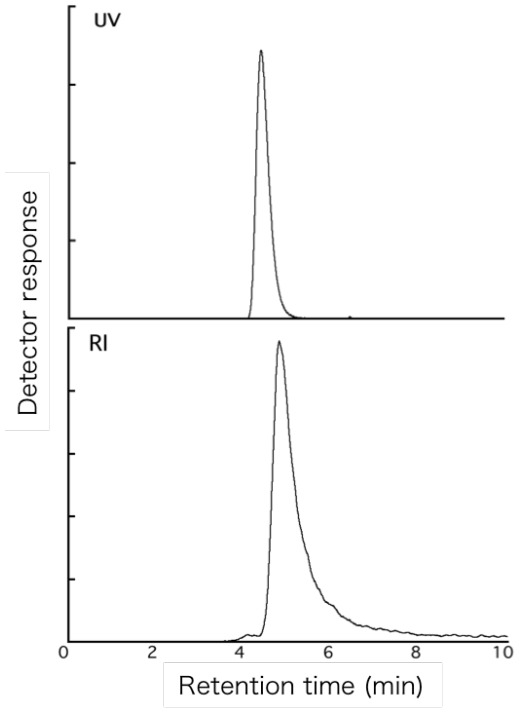


Fig. 4.1 High-performance liquid chromatography chart of $^{211}$At-trastuzumab.

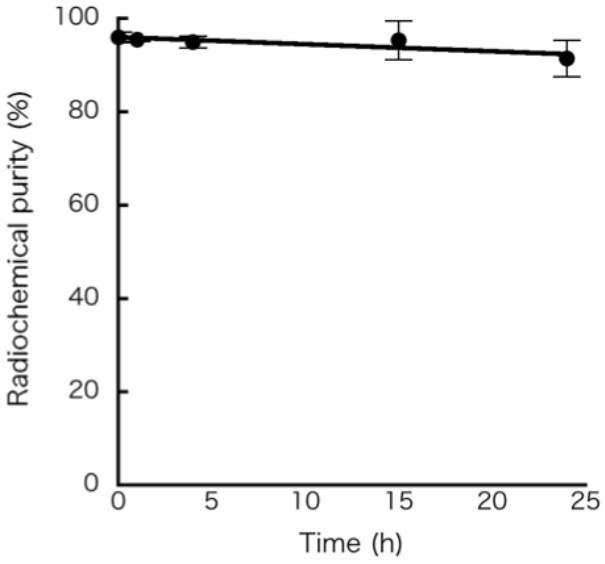


Fig. 4.2 Serum stability of $^{211}$At-trastuzumab up to 24 h incubation in murine serum, evaluated with RPC by methanol precipitation. Two independent experiments were performed in duplicate (n=2). Data represent mean ± SD.

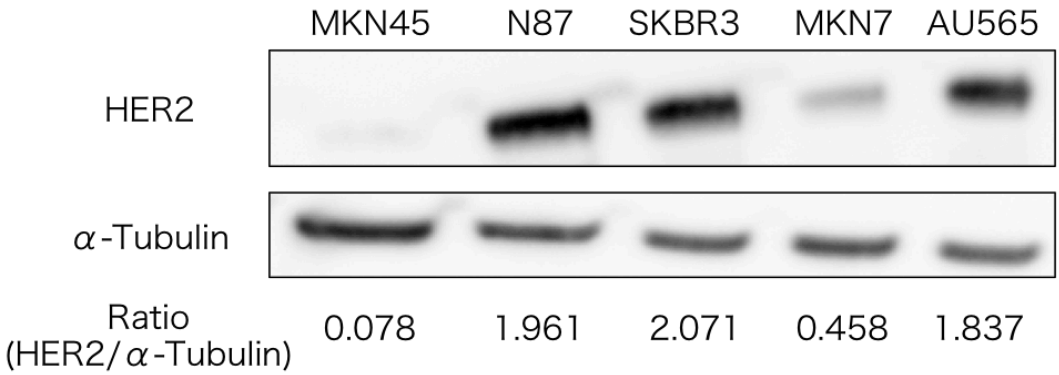


Fig. 4.3 HER2 expressions of MKN45, N87, SKBR3, MKN7 and AU565 cells. α-tubulin as loading control. Ratios of bind intensity of HER2 relative to α-tubulin are indicated below the images.

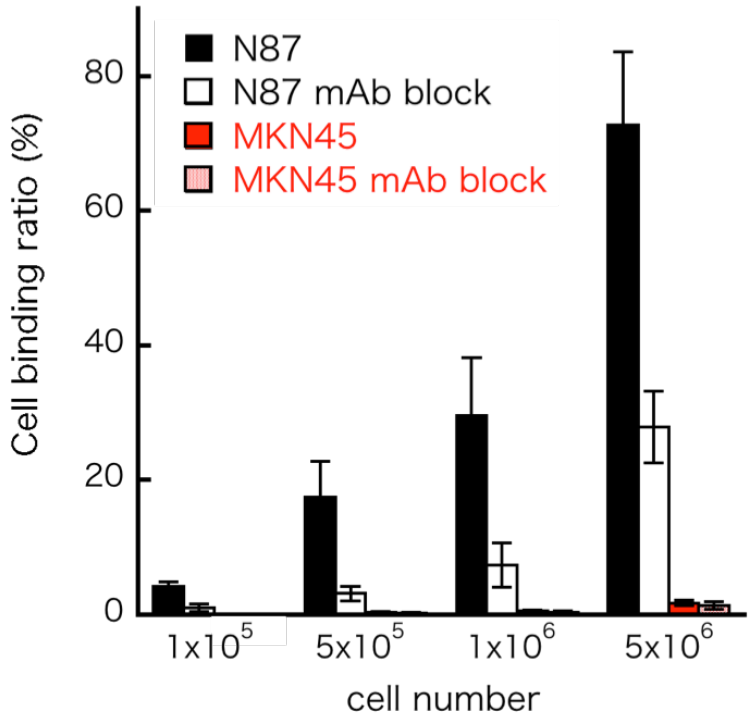


Fig. 4.4 Cell binding ratio of $^{211}$At-trastuzumab to N87 and MKN45 cells with/without trastuzumab (mAb) block. Bar legends are indicated in the graph. Three independent experiments were performed in triplicate (n=3).

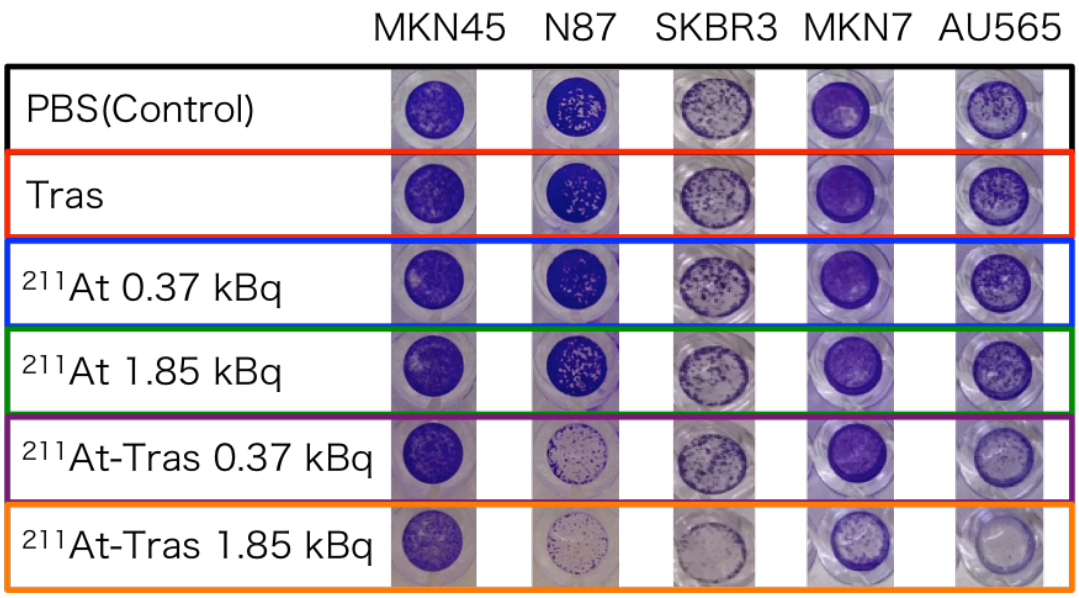


Fig. 4.5 A representative image of stained survived cells after 7 d post 24 h treatment with PBS control, trastuzumab (Tras), $^{211}$At (0.37, 1.85 kBq) or $^{211}$At-trastuzumab ($^{211}$At-Tras; 0.37, 1.85 kBq).

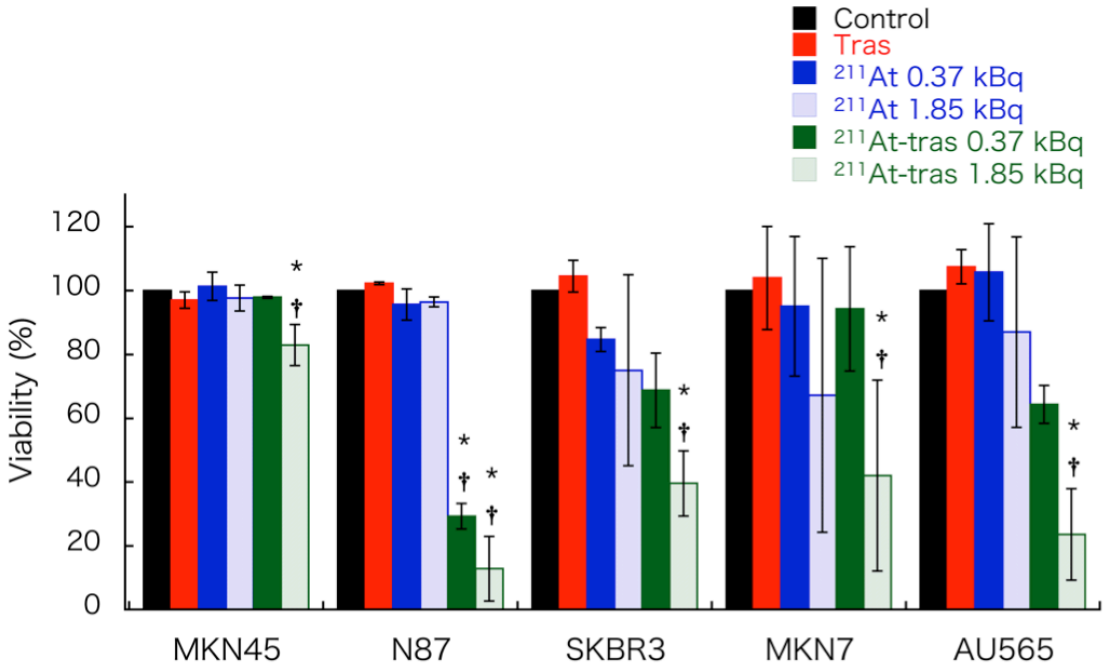


Fig. 4.6 Quantification of the cell viability in cells treated with $^{211}$At-trastuzumab for 7 d. Results in Figure 4.5 are quantified. Bar legends are indicated in the graph. Three independent experiments were performed in triplicate (n=3). All data represent mean ± SD ($P<0.05$, *vs Control, †vs Tras)

### 4.2 $^{211}$At-trastuzumab shows antitumor activity against s.c. xenografts of HER2-positive GC cells.

To investigate the potential antitumor activity of $^{211}$At-trastuzumab against human GC cells in vivo, we examined the antitumor effects of $^{211}$At-trastuzumab in nude mice bearing s.c. N87 tumors (Fig. 4.8; 4.9). Prior to treatment, the tissue uptake of $^{211}$At was measured to analyze the biodistribution of $^{211}$At-trastuzumab (0.5 MBq) in s.c. xenografts. This biodistribution analysis revealed that the uptake of i.v. injected $^{211}$At-trastuzumab increased in the s.c. tumor over time, peaking at approximately 12.5 ± 4.0%ID/g at 24 h after the injection (Fig. 4.7). The spleen showed the highest uptake (23.7 ± 8.6%ID/g) in all tissues at 1 h post-injection, which decreased over time to 7.0 ± 1.9%ID/g after 24 h. The uptake in the whole blood peaked at 3 h after injection (27.1 ± 4.7%ID/g) and decreased thereafter. Uptake of $^{211}$At-trastuzumab in the thyroid and stomach remained high, even at 24 h post-injection (14.3 ± 8.4%ID/g and 18.0 ± 8.1%ID/g, respectively).

To evaluate its therapeutic efficacy in s.c. HER2-positive GC xenografts, a single dose of $^{211}$At-trastuzumab (0.1 or 0.5 MBq) was i.v. injected into mice bearing an s.c. N87 xenograft. An equivalent protein amount of unlabeled trastuzumab and PBS were injected as controls. There was no significant difference in the relative tumor volume between the control and trastuzumab-treated mice (Fig. 4.8). Both groups treated with 0.1 or 0.5 MBq $^{211}$At-trastuzumab showed a significant suppression of tumor growth compared with the PBS control group ($P < 0.05$) and the 0.5 MBq $^{211}$At-trastuzumab dose significantly suppressed tumor growth compared with unlabeled trastuzumab ($P < 0.05$) (Fig. 4.8). Mice treated with 0.1 or 0.5 MBq $^{211}$At-trastuzumab had a significantly prolonged median survival (52 and >84 days, respectively) compared with the PBS and unlabeled trastuzumab treated controls (38 and 31 days, respectively; Fig. 4.9). No significant differences were found in the bodyweights among any of the treatment groups (Fig. 4.10). The white blood cell counts sharply decreased only in the mice injected with 0.5 MBq $^{211}$At-trastuzumab and recovered

after 3 weeks (Fig. 4.11).

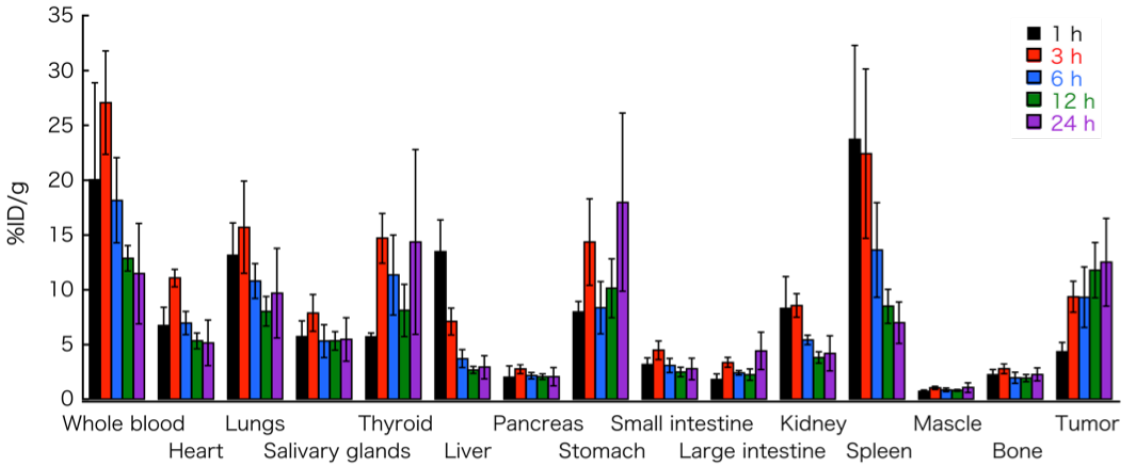


Fig. 4.7 Biodistribution of $^{211}$At-trastuzumab in mice with subcutaneous xenograft of N87. Uptakes (%ID/g) of $^{211}$At in tumor and other organs at 1, 3, 6, 12, 24-h after intravenous injection of $^{211}$At-trastuzumab (0.5 MBq). 4 mice were used for all each time point. All data represent mean ±SD.

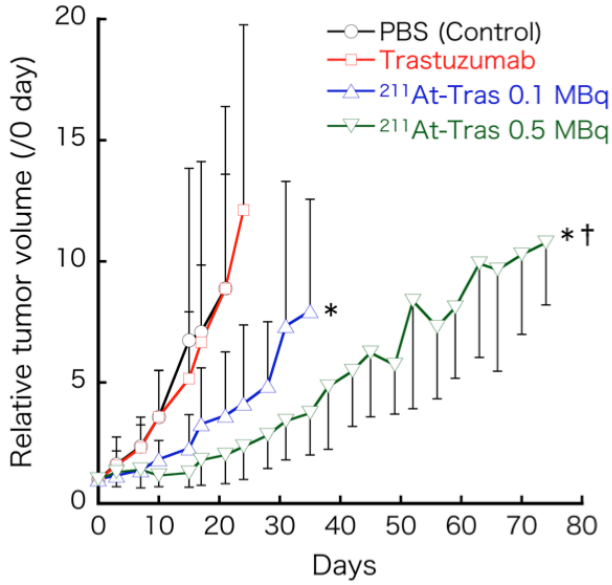


Fig. 4.8 Relative tumor volume in each mouse enrolled in this study. Tumor volume before the treatment was considered as 100%. 6 mice were enrolled to all of the treatment groups but trastuzumab (7 mice). All plots were interrupted when one mouse enrolled reached endpoint. All data represent mean ±SD (P<0.05, *vs Control, †vs Tras).

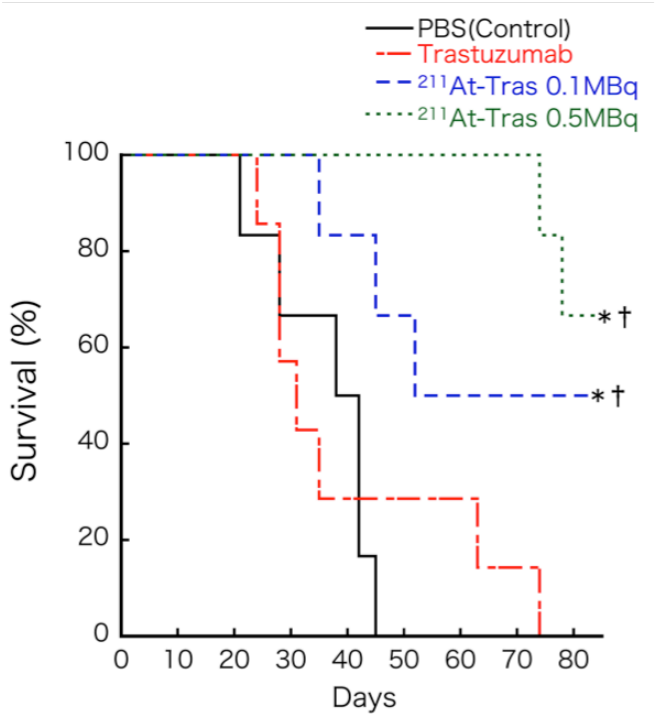


Fig. 4.9 Kaplan-Meier survival curves of s.c. mice (P<0.05, *vs Control, †vs Tras).

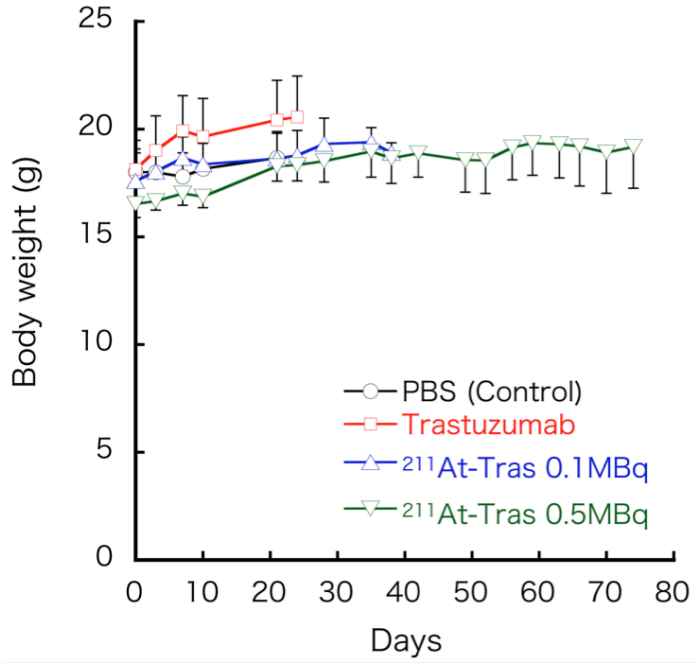


Fig. 4.10 Body weight of mice after treatment. All plots were interrupted when one mouse enrolled reached endpoint. All data represent mean ±SD.

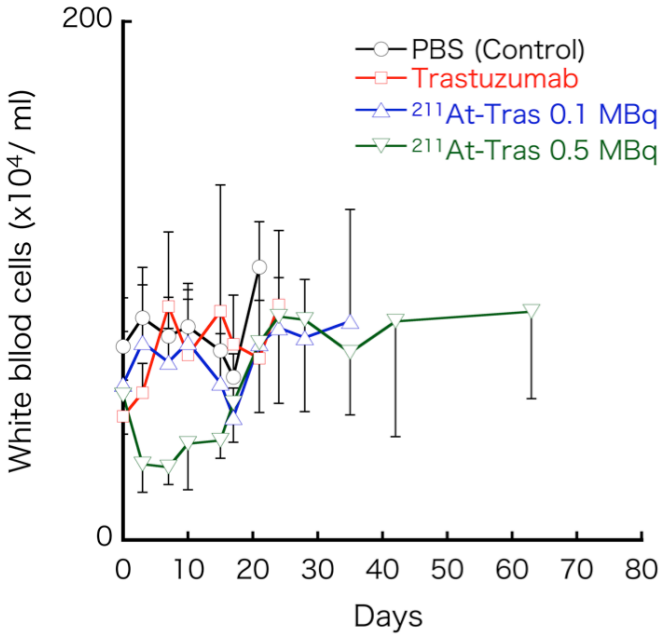


Fig. 4.11 The number of white blood cell of mice after treatment. All plots were interrupted when one mouse enrolled reached endpoint. All data represent mean ±SD.

**4.3 Establishment of a xenograft mouse model of PMGC.**

We established a xenograft mouse model of PMGC that allowed tumor growth to be monitored by in vivo bioluminescence imaging (Figs. 4.13). N87/Luc cells, which are N87 cells that stably express luciferase, were generated by lentiviral infection (Fig. 4.12). The bioluminescence activity of the N87/Luc cells correlated well with the cell number (Fig. 4.12a,b). The level of HER2 expression in the N87/Luc cells was nearly equivalent to that in N87 cells (Fig. 4.12c). A mouse model of PMGC was generated by i.p. injection of N87/Luc into SCID mice (Fig. 4.13). Peritoneal metastasis of GC could be seen around the liver, pancreas, and peritoneal region by in vivo bioluminescence imaging (Fig. 4.13a–c). Human epidermal growth factor receptor 2 was found to be strongly expressed in xenograft tumors in PMGC mice (Fig. 4.13d).

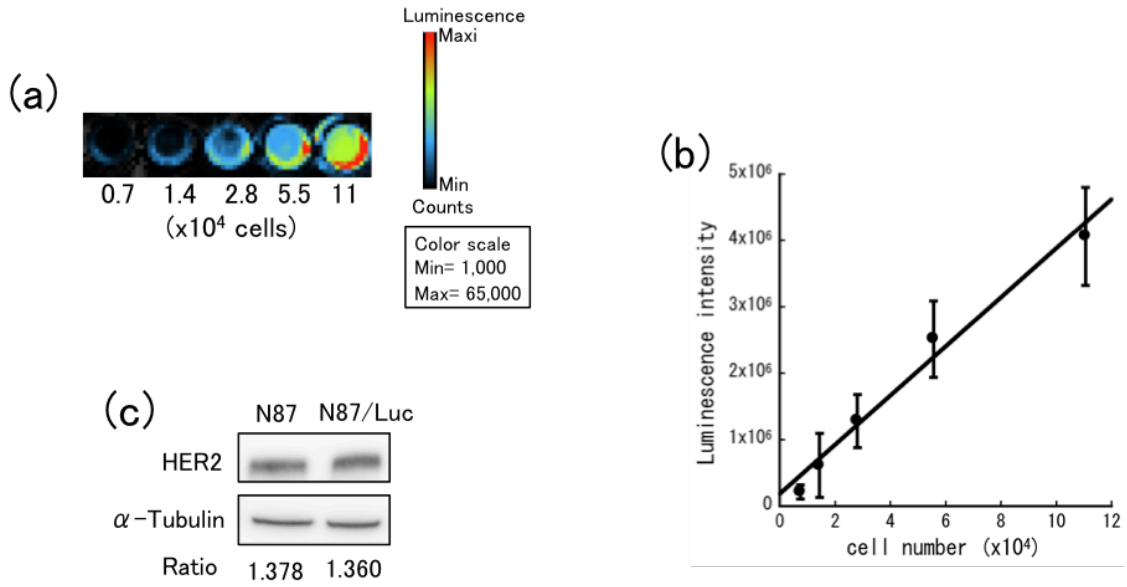


Fig. 4.12 Establishment of N87/Luc cells.

(a) Representative immunofliorescemce images of concentrations of N87/Luc cells (0.7-11 x $10^4$ cells) after 10 min incubation of luciferin(10mg/ml, 50 µl/well) . (b) Quantified data of (a). Experiment was performed in quadruple. Data represent mean ±SD. (c) HER2 expressions of N87 and N87/Luc cells. α-tubulin as loading control. Ratios of bind intensity of HER2 relative to α-tubulin are indicated below the images. The band of N87 is same with Fig. 4.3.

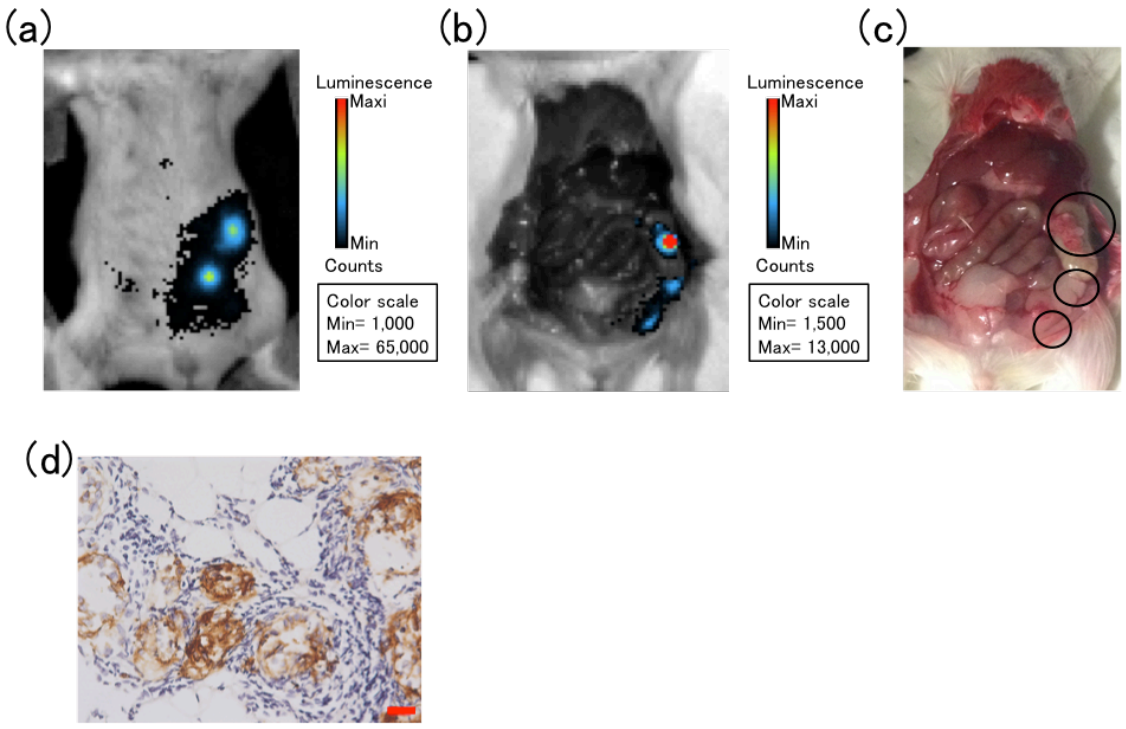


Fig. 4.13 Establishment of PMGC xenofraft mouse models.

(a) Representative chemiluminescence images of PM in the PMGC xenofraft mouse models captured 10 min after injection of luciferin with abdomen closed. A color scale is indicated luminescence intensity per pixel (Min=1,000, Maxi=65,000). Representative, same mouse with (a), (b) chemiluminescence and (c) visual images of PM in the PMGC xenofraft mouse models captured 20 min after injection of luciferin with abdomen opened. A color scale is indicated luminescence intensity per pixel (Min=1,500, Maxi=13,000). Circles highlight visible tumor lesion (c). (d) HER2 immunohistochemical staining of PMGC dissected from xenograft mouse model. Scale bar = 20μm.

### 4.4 More efficient delivery of $^{211}$At-trastuzumab to PMGC with i.p. rather than i.v. injection.

To optimize the system of delivery of $^{211}$At-trastuzumab to PMGC in our mouse model, we measured the tumor uptake of $^{211}$At in HER2-positive PMGC mice in order to compare the biodistribution of $^{211}$At-trastuzumab between i.p. and i.v. injected animals (Fig. 4.14). $^{211}$At-trastuzumab (1 MBq) was injected into the mice either by i.p. or i.v. routes, and the major tissues, including the PMGCs, were sampled at different time points. The maximum tumor uptake of $^{211}$At in the i.p. group was 63.9 ± 52.6%ID/g at 3 h, whereas it was 18.1 ± 8.6%ID/g at 12 h in the i.v. group. The overall uptakes in the whole blood and spleen were also lower in the i.p. group than in the i.v. group. These data suggest that i.p. injection more efficiently delivers $^{211}$At-trastuzumab to HER2-positive PMGCs without an undesirable distribution to other tissues.

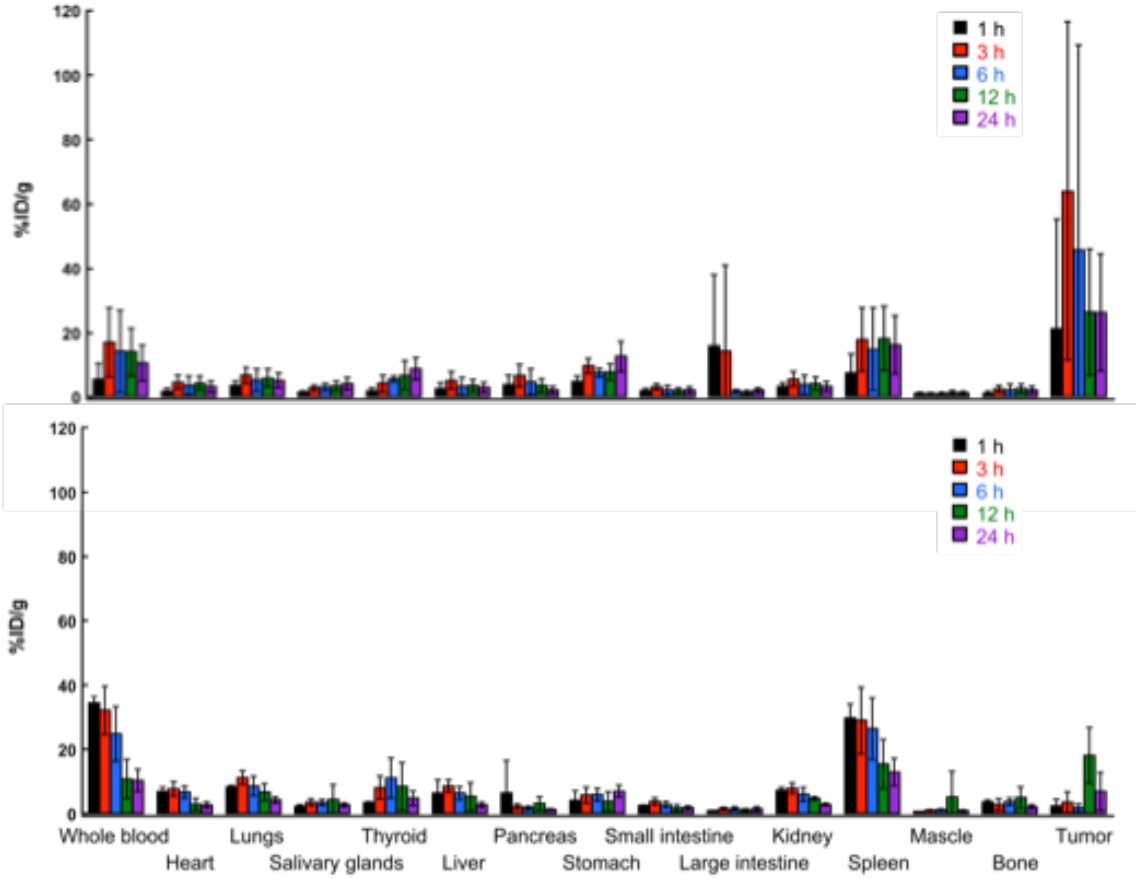


Fig. 4.14 Biodistribution of $^{211}$At-trastuzumab in mice with peritoneal metastasis of N87. Uptakes (%ID/g) of $^{211}$At in tumor and other organs at 1, 3, 6, 12, 24-h after intraperitoneal (upper) or intravenous (bottom) injection of $^{211}$At-trastuzumab (1 MBq). Five mice (for intraperitoneal injection) or 4 mice (for intravenous injection) were used for all each time point. All data represent mean ±SD.

**4.5 Locoregionally administered $^{211}$At-trastuzumab efficiently treats HER2-positive PMGC in a mouse model.**

We evaluated the therapeutic efficacy of $^{211}$At-trastuzumab against HER2-positive PMGC in our mouse model (Figs. 4.15; Fig. 4.16; Table 1). The PMGC mice received a single i.p. injection of PBS, unlabeled trastuzumab, free $^{211}$At (1 MBq), or $^{211}$At-trastuzumab (0.1 or 1 MBq) 8 days after N87/Luc implantation. The tumor growth was monitored longitudinally in each group by in vivo bioluminescence imaging (Fig. 4.15a). Representative bioluminescence images of the mice from each group are shown in Figure 4.15(b). Tumor growth was evident in the PMGC mice injected with PBS, unlabeled trastuzumab, free $^{211}$At, and 0.1 MBq $^{211}$At-trastuzumab. In contrast, a single injection of 1 MBq $^{211}$At-trastuzumab reduced the tumor burden at 3 weeks after injection, with the tumors becoming undetectable at 5–7 weeks after treatment. The relative bioluminescence signal changes in the tumors in all of the treated PMGC mice are shown in Figure 16(a). Trastuzumab and PBS injections had little to no effect on tumor growth in the PMGC model. Tumor growth appeared to be stable until 20 days after treatment with free $^{211}$At and resumed thereafter. In PMGC mice treated with 0.1 MBq $^{211}$At-trastuzumab, some mice appeared to have stable disease but ultimately showed disease recurrence. However, in five of the six mice treated with 1 MBq $^{211}$At-trastuzumab, the tumors shrank or stopped growing from 4 days after treatment and had disappeared or were still growth arrested at 60 days after treatment. Only a single mouse that received a 1-MBq dose of $^{211}$At-trastuzumab showed tumor growth, which was possibly due to misinjection. The therapeutic results of $^{211}$At-trastuzumab in the PMGC model are presented in Table 1. All mice treated with PBS control, unlabeled trastuzumab, and $^{211}$At (1 MBq) showed tumor progression and reached the endpoint (a tumor luciferase intensity of $1.5 \times 10^7$) within 60 days of treatment. Two of the six mice that received 0.1 MBq $^{211}$At-trastuzumab showed a 50% reduction in the tumor but eventually also reached the endpoint. Two of the six mice that received a 1-MBq dose of

$^{211}$At-trastuzumab had undetectable tumors; a further three of these mice showed a 50% or 90% tumor reduction, and one mouse still showed tumor growth. The five mice showing tumor regression had not reached the endpoint by 60 days after treatment. Not surprisingly, survival was significantly prolonged in the 1 MBq $^{211}$At-trastuzumab group compared with all of the other groups ($P < 0.05$). The median survival outcomes were 26, 29, 50, and 43 days in the PBS control, unlabeled trastuzumab, 1 MBq $^{211}$At, and 0.1 MBq $^{211}$At-trastuzumab groups, respectively (Fig. 17).

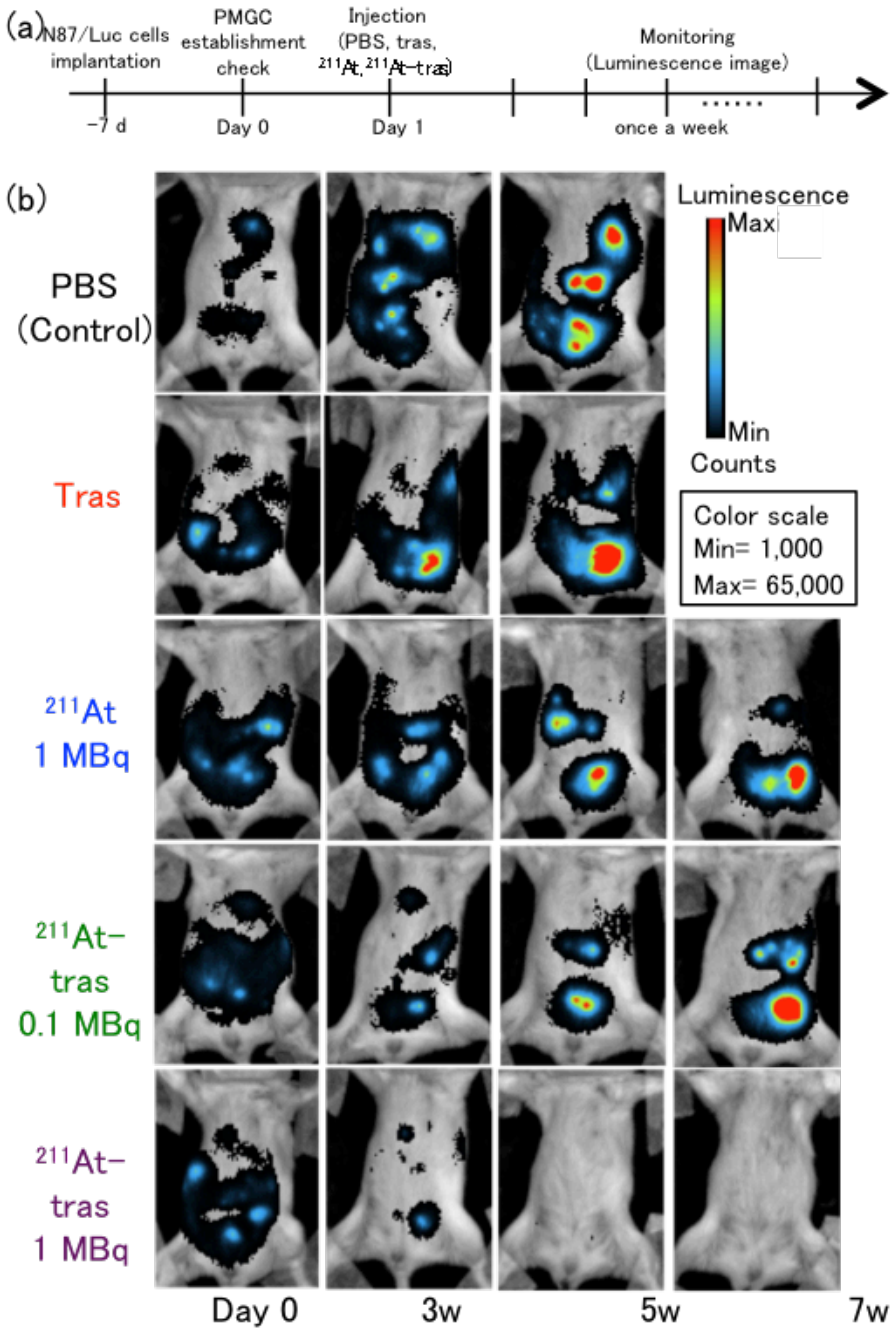


Fig. 4.15 (a) Experiment time curse of radioimmunotherapy to PMGC mouse model. (b)Representative chemiluminescence images of tumor growth in the peritoneal metastasis mouse models treated with PBS (Control), trastuzumab (Tras), $^{211}$At (1 MBq), or $^{211}$At-trastuzumab ($^{211}$At-Tras; 0.1 or 1 MBq). Shown are images the day before the treatment and 3, 5, 7 w after treatment. A color scale is indicated luminescence intensity per pixel (Min=1,000, Maxi=65,000).

Table 1 Tumor response after treatment

| Treatment groups | Undetectable tumor * | 50% reduction † | 90% reduction ‡ | Progressing tumors | No. of survivors § |
|---|---|---|---|---|---|
| PBS(Control) (n=5) | 0/5 | 0/5 | 0/5 | 5/5 | 0/5 |
| Tras (n=6) | 0/6 | 0/6 | 0/6 | 6/6 | 0/6 |
| 211At 1 MBq (n=6) | 0/6 | 0/6 | 0/6 | 6/6 | 0/6 |
| 211At-tras 0.1 MBq (n=6) | 0/6 | 2/6 | 0/6 | 4/6 | 0/6 |
| 211At-tras 1 MBq (n=6) | 2/6 | 2/6 | 1/6 | 1/6 | 5/6 |

Table 1 Tumor response up to 60 d after treatment in the peritoneal metastasis mouse models treated with PBS (Control), trastuzumab (Tras), $^{211}$At (1 MBq), or $^{211}$At-trastuzumab ($^{211}$At-Tras; 0.1 or 1 MBq). * : The number of mice, which the PMGC was undetectable once. †, ‡: The number of mice, which the total luminescence intensity of PMGC was reduced to 50 and 90%, respectively. §: The number of mice, which the total luminescence intensity of PMGC did not reach the endpoint (1.5 x $10^7$).

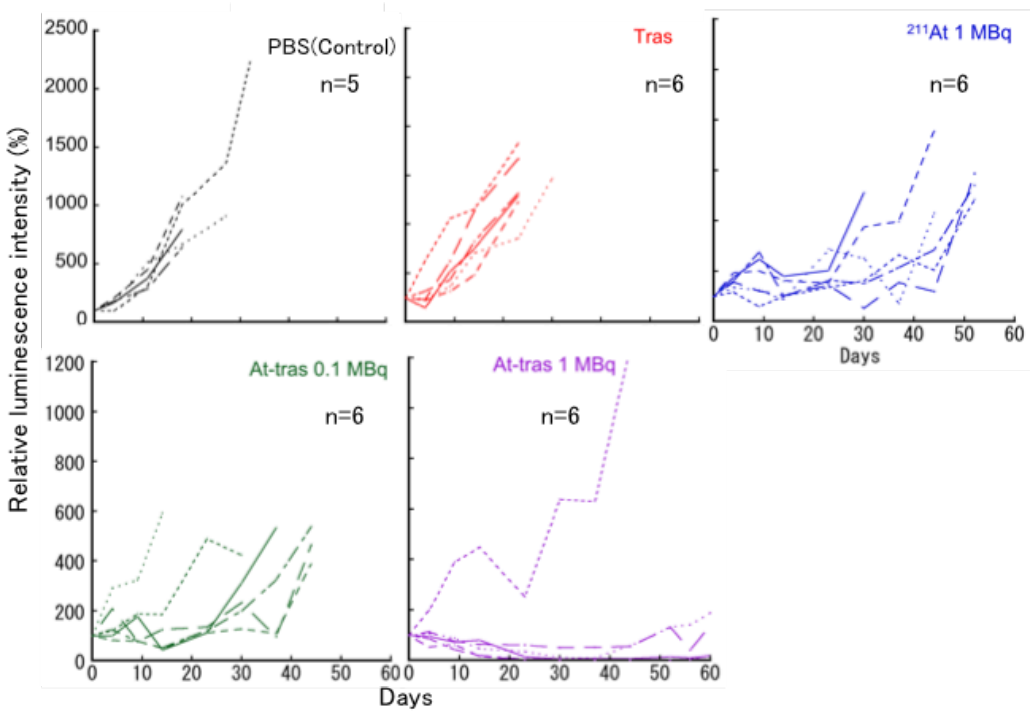


Fig. 4.16 Quantified relative tumor luminescence intensity in each mouse enrolled in this study. Luminescence intensity before the treatment was considered as 100%. 6 mice were enrolled to all of the treatment groups but control (5 mice).

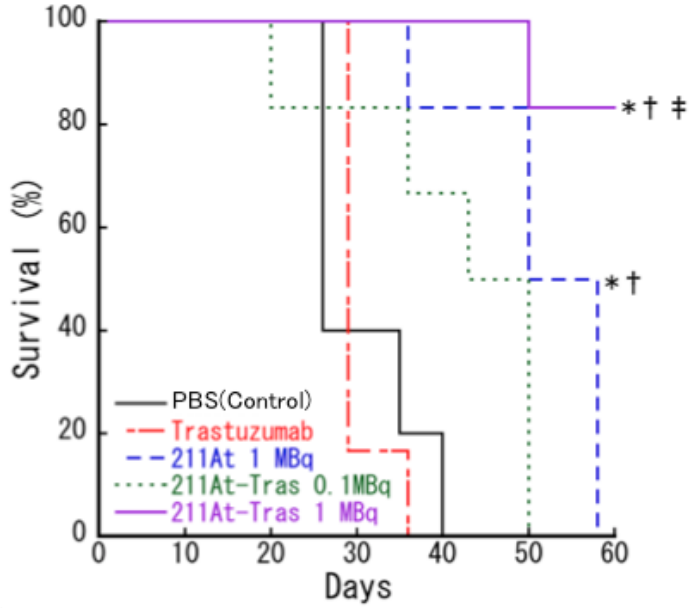


Fig. 4.17 Kaplan-Meier survival curves of mice (P<0.05, *vs Control, †vs Tras, ‡vs $^{211}$At).

### 4.6 Excretion and adverse effects of i.p. injected $^{211}$At-trastuzumab in PMGC mouse model.

To evaluate the possible adverse effects of $^{211}$At-trastuzumab in our PMGC model, we monitored whether any changes occurred in the bodyweight or number of leukocytes in the treated mice. No apparent bodyweight loss was evident in any of the treated groups during the observation period (Fig. 4.18). In addition, no leukocytopenia was found in any of the groups, including the 1 MBq $^{211}$At-trastuzumab mice (Fig. 4.19). To then assess the excretion of $^{211}$At from the body, we measured its levels in feces and urine. The total $^{211}$At activity in the urine (7.3%ID) of the PMGC mice up to 24 h post i.p. injection of $^{211}$At-trastuzumab was much higher than that in the feces (1.3%ID) (Fig. 4.20). Biochemical examination of glutamic oxaloacetic transaminase, glutamic pyruvate transaminase, and blood urea nitrogen at 1, 7, and 14 days post-injection revealed no significant change compared to the pre-treatment level (Fig. 4.21). Creatinine was not detected in any of the mice preinjection or at 1, 7, or 14 days post-injection.

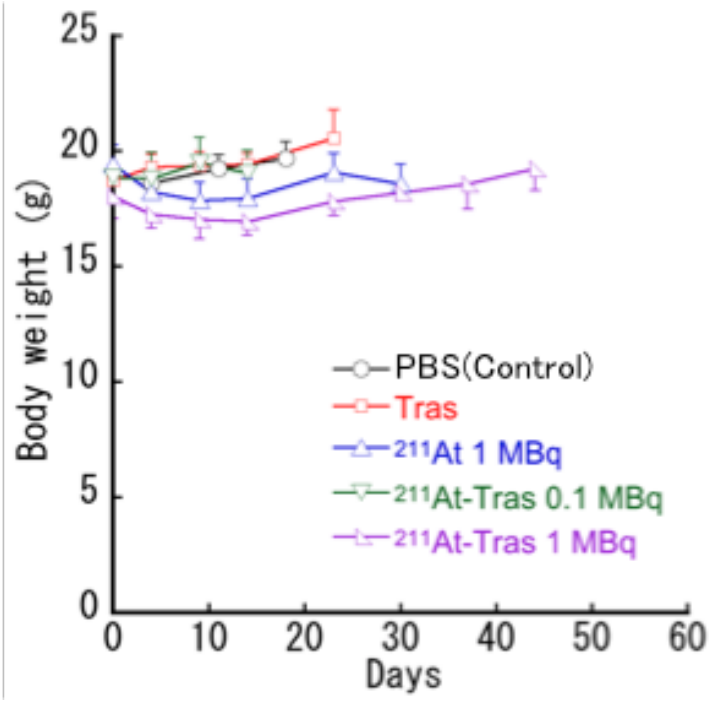


Fig. 4.18 Body weight of mice after treatment. Plots were interrupted when one mouse enrolled reached endpoint. Data represent mean ±SD.

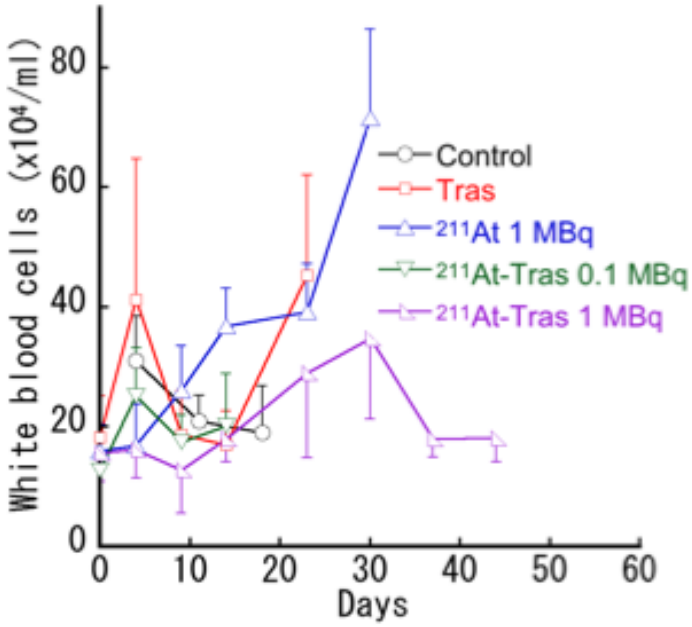


Fig. 4.19 The number of white blood cell of mice after treatment. Plots were interrupted when one mouse enrolled reached endpoint. Data represent mean ±SD.

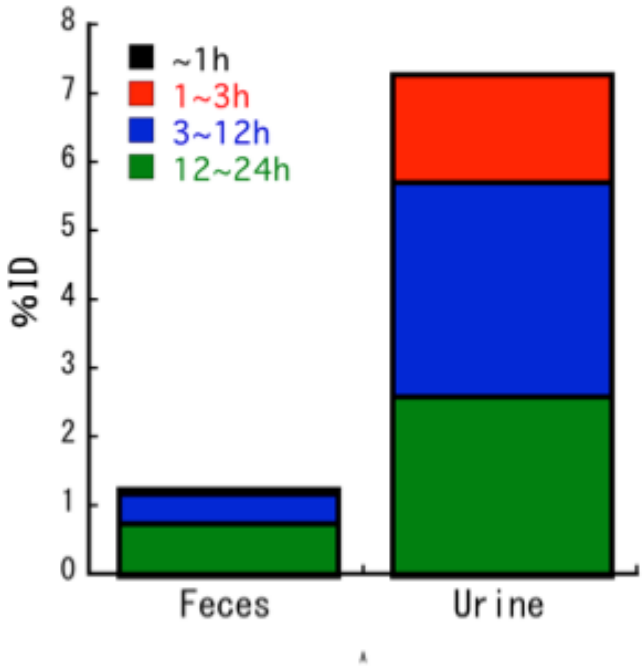


Fig. 4.20 The activities of $^{211}$At in both feces and urine of PMGC model mice up to 24 h after i.p. injection of $^{211}$At-tras (1 MBq). Six mice were used for the experiment (n=6) and data represent mean. Bar legends are indicated in the graph.

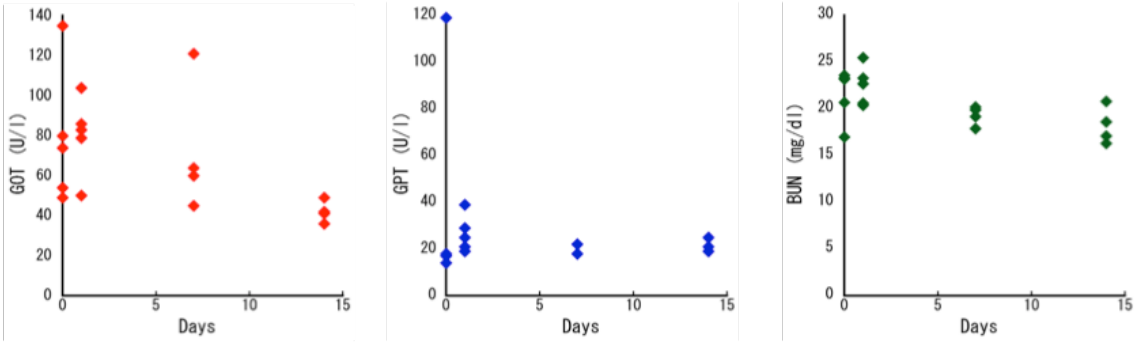


Fig. 4.21 The data of biochemical examination of GOT (red), GPT (blue) and BUN (green) up to 14 d after injection of i.p. $^{211}$At-tras (1 MBq). Five mice were used for 0 and 1 d, and four mice were used for 7 and 14 d. The data of each mouse are shown in the graph.

**4.7 DNA damage is induced in tumor cells by $^{211}$At-trastuzumab.**

To better understand how $^{211}$At-trastuzumab kills tumor cells, we examined the DNA damage in these cells both in vitro and in vivo by detecting γH2AX foci using immunostaining and Western blot analysis. Clusters of γH2AX foci were clearly observed in N87 cells treated with $^{211}$At-trastuzumab for 24 h, but barely detectable in N87 cells treated with PBS or unlabeled trastuzumab (Fig. 4.22). In addition, MKN45 cells treated with even the maximum dose of $^{211}$At-trastuzumab (37 kBq) showed barely any γH2AX foci (Fig. 4.22). The level of γH2AX, evaluated by Western blotting, also showed a clear dose-dependency and increased in N87 cells treated with $^{211}$At-trastuzumab compared to PBS and unlabeled trastuzumab (Fig. 4.22). A slightly increased level of γH2AX was observed in MKN45 cells with a high-dose treatment of $^{211}$At-trastuzumab (18.5 and 37 kBq), but was still much lower than that in N87 cells (Fig. 4.22). Dense clusters of γH2AX foci could clearly be observed in N87 cells treated with 18.5 kBq $^{211}$At-trastuzumab after 24 h in an immunofluorescence image taken at a higher magnification (Fig. 4.22). Clusters of γH2AX foci were clearly evident in tumors dissected from the PMGC model mice at 6 h after the i.p. injection of 1 MBq $^{211}$At-trastuzumab, compared to the control and unlabeled trastuzumab-treated animals (Fig. 4.23). As shown in Figure 4.23, clusters of γH2AX foci were located in the same area showing HER2 expression (Fig. 4.23). These observations indicate that $^{211}$At-trastuzumab specifically induces DNA DSBs in HER2-positive PMGC cells.

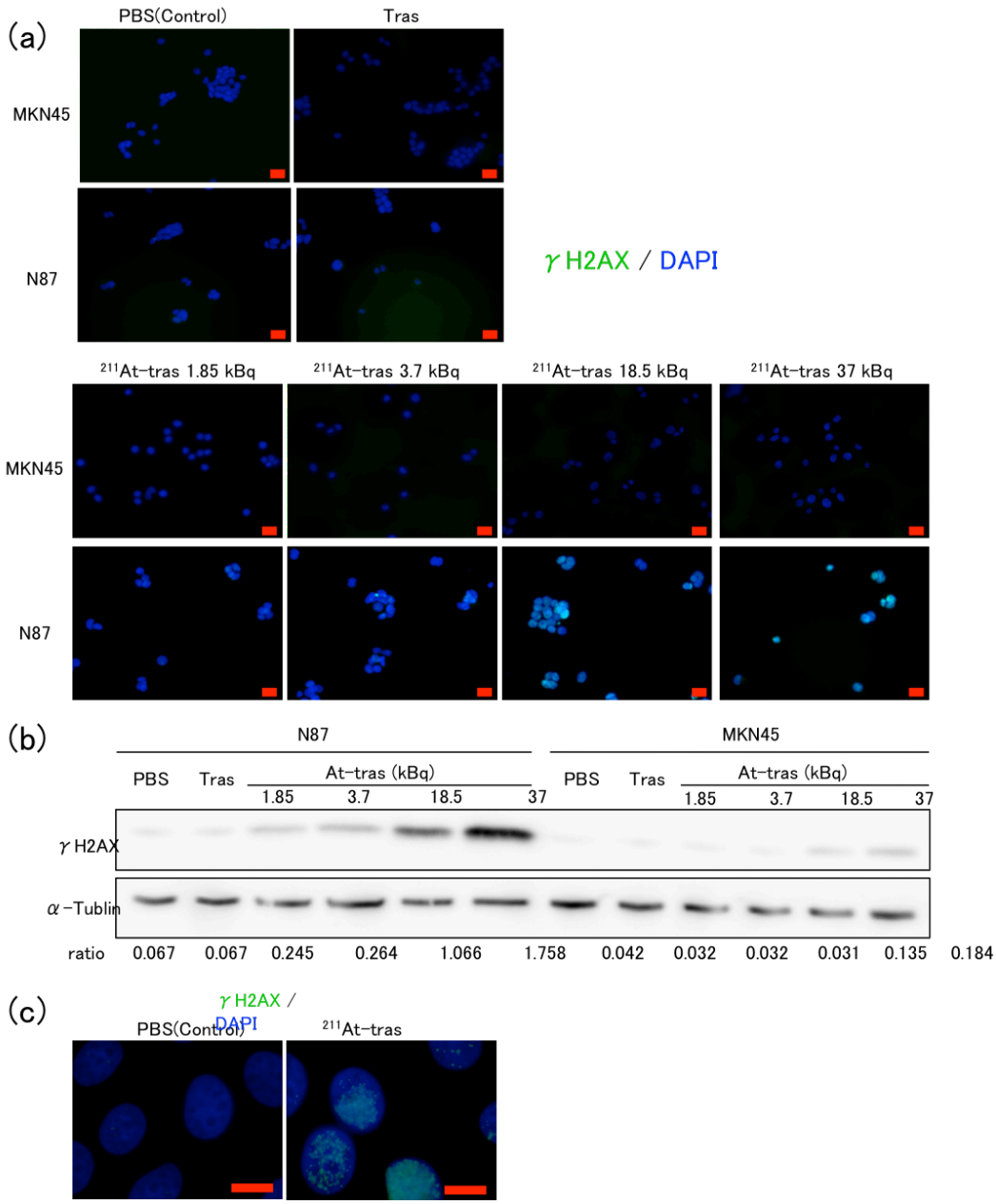


Fig. 4.22 Representative immunofliorescemce images of γH2AX foci in GC cells after treated with $^{211}$At-trastuzuma. (a) γH2AX foci in MKN45 and N87 cells treated with either PBS, Tras or $^{211}$At-trastuzumab (1.85, 3.7, 18.5, 37 kBq). Scale bar = 20μm. (b) γH2AX expressions in N87 and MKN45 cells treated with either PBS, Tras or $^{211}$At-trastuzumab (1.85, 3.7, 18.5, 37 kBq). α-tubulin as loading control. Ratios of bind intensity of γH2AX relative to α-tubulin are indicated below the images. (c) γH2AX foci in N87 cells treated with either PBS or 18.5 kBq of $^{211}$At-trastuzumab. Scale bar = 10μm.

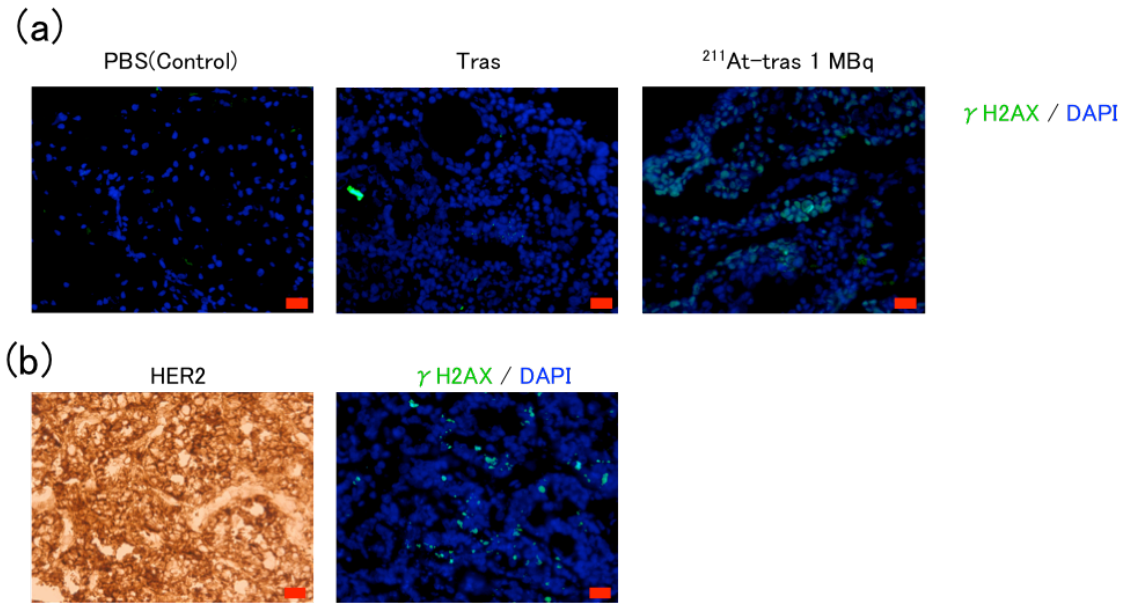


Fig. 4.23 Representative immunofliorescemce images of γH2AX foci in PMGC after treated with $^{211}$At-trastuzumab. (a) γH2AX foci in PMGC after 6 hour injected PBS, Tras or 1 MBq of $^{211}$At-trastuzumab. Scale bar = 20μm. (b) HER2 and γH2AX foci in PMGC after 3 hour injected treated 1 MBq of $^{211}$At-trastuzumab. Scale bar = 20μm.

# 5． Discussion

Despite recent advances in chemotherapy and molecular targeted therapies directed against advanced GC, the prognosis of patients with PMGC is still miserably poor. In our current study, we show that $^{211}$At-trastuzumab specifically targets HER2-positive GC cells, both in vivo and in vitro, and successfully inhibits tumor growth and improves survival in PMGC model mice. Our in vitro cytotoxicity analyses showed that $^{211}$At-trastuzumab specifically kills HER2-positive cells, but not MKN45 cells that have little expression of HER2. Free $^{211}$At had little effect in either cell type in vitro. Given that radiolabeled trastuzumab is internalized into the cells it binds,(8) our present data suggest that targeted cell binding and internalization of $^{211}$At-trastuzumab is required for $^{211}$At to exert its cytotoxic effects. A specific targeting strategy is critically important to maximize the cell-killing effects of α-particle emitters in α-RIT.

We clearly found from our current experiments that i.p. administration is superior to i.v. injection in delivering $^{211}$At-trastuzumab to tumors disseminated in the peritoneal cavity. Considering that $^{211}$At decays with a half-life of 7.2 h, a faster accumulation of high-dose $^{211}$At to the target lesion is required to maximize its antitumor effects. Intraperitoneal delivery also resulted in a lower distribution of $^{211}$At to other normal tissues, including the whole blood and spleen, compared with i.v. injection. These data strongly suggest that locoregional therapy helps to avoid adverse effects. Moreover, in this regard, we found that an i.v. injection of $^{211}$At-trastuzumab (0.5 MBq) resulted in acute but recoverable leukocytopenia in s.c. xenografts.

In contrast, no leukocytopenia or bodyweight loss was evident in i.p. injected mice, even those injected with a 1-MBq dose of $^{211}$At-trastuzumab. In addition, no significant biochemical changes in either the liver or kidney were observed in mice treated with 1 MBq $^{211}$At-trastuzumab. We conclude, therefore, that i.p. delivery of $^{211}$At-trastuzumab is far more suitable in terms of undesirable adverse effects. Recent studies have explored the

utility of i.p. α-RIT in various preclinical cancer models.(16–18) Furthermore, a previous clinical trial reported that the therapeutic absorbed dose of i.p. a-RIT in ovarian cancer at the peritoneal cavity was >100 times greater than that in the red bone marrow without significant toxicity.(19) Thus, i.p. a-RIT appears to be a clinically feasible approach.

We further showed from our current analysis that a-RIT with $^{211}$At-trastuzumab suppressed tumor growth in both s.c. GC xenografts and PMGC xenografts. In our PMGC mice, five of the six that received only a single locoregional treatment with $^{211}$At-trastuzumab showed improved survival and a drastic reduction in tumor burden. We also found that $^{211}$At-trastuzumab induced massive DNA DSBs in HER2-positive GC cells, but not in HER2-negative cells. Unlabeled trastuzumab of an equal protein level to that of the labeled antibody could not induce DSB in N87 cells. We thus speculate that α-particles emitted from $^{211}$At-trastuzumab efficiently induced irreparable DSBs in N87 cells and thereby caused tumor shrinkage.

A previous study showed that $^{211}$At-trastuzumab is effective against radioresistant ovarian i.p. tumors in mice.(20) In that report, a single i.p. injection of 0.8 MBq $^{211}$At-trastuzumab did not achieve a tumor-free outcome in the mice. However, 0.4 MBq radiolabeled antibody combined with unlabeled trastuzumab resulted in a complete eradication of the tumors. Additionally, 500 μg unlabeled trastuzumab, which is a more than 100-fold higher amount of protein than that used in our present experiments, had a better therapeutic result compared to 0.8 MBq $^{211}$At-trastuzumab monotherapy. In the present study, we did not fully investigate the effects of unlabeled trastuzumab on human GC N87 cells. Further studies are therefore needed to clarify the effects of unlabeled antibody on a-RIT.

The success of trastuzumab has led us to develop a novel type of HER2-targeted drug. Previously, trastuzumab emtansine, an antibody–drug conjugate carrying the cytotoxic agent emtansine bound to trastuzumab, has shown antitumor activity against HER2-positive tumors and emerged

as a powerful therapeutic option for advanced or metastatic breast cancer that is resistant to trastuzumab.(21,22) We speculate, however, that because a single α-particle atom can kill a target cell,(11,12) the cytotoxic effects of $^{211}$At-trastuzumab could even be superior to those of trastuzumab-based antibody–drug conjugates.

In principle, locoregional α-RIT reduces the risk of the hematological toxicities that are the most worrying adverse effects of this treatment approach.

# 6． Conclusion

We propose that locoregional α-radioimmunotherapy using $^{211}$At-trastuzumab is a safe and highly effective therapy and is a very promising future therapeutic option for PMGC.

# 7． Acknowledgments

I thank Drs. Sumitaka Hasegawa, Kotaro Nagatsu, Tadashi Kamada and Ms. Yukie Morokoshi for the great contribution for this research. I also thank Drs. Tsuneo Saga, Takako Furukawa, Atsushi Tsuji, and Masumi Abe for helpful discussions and support, and Katsuyuki Minegishi and Hisashi Suzuki for radioisotope production. This work was partly supported by the Japan Society for the Promotion of Science (KAKENHI Grant Nos. 24390296 to S.H., 16H07460 to Y.M., and 17J02307 to H.K.L.), a research grant from the Astellas Foundation for research on metabolic disorders (to S.H.), and a President's grant from the National Institute of Radiological Sciences (to S.H.).

# 8. Abbreviations

| | |
|---|---|
| $^{211}$At | astatine-211 |
| $^{209}$Bi | bismuth-209 |
| DNA | deoxyribonucleic acid |
| DSB | double-strand break (in the DNA macromolecule) |
| GC | gastric cancer |
| HER2 | human epidermal growth factor receptor-2 |
| i.p | intraperitoneal(ly) |
| i.v. | intravenous(ly) |
| LET | linear energy transfer |
| NCS | N-Chlorosuccinimide |
| m-MeATE | N-Succinimidyl-3-(trimethylstannyl)benzoate |
| PBS | phosphate buffered saline |
| %ID/g | percent injected dose per gram of tissue |
| PMGC | peritoneal metastasis of gastric cancer |
| RIT | radioimmunotherapy |
| SPECT | single photon emission computed tomography |
| s.c. | subcutaneous(ly) |

# 9. References


1 Karimi P, Islami F, Anandasabapathy S, Freedman ND, Kamangar F. Gastriccancer: descriptive epidemiology, risk factors, screening, and prevention.Cancer Epidemiol Biomarkers Prev 2014; 23: 700–13.

2 Thomassen I, van Gestel YR, van Ramshorst B et al. Peritoneal carcinomatosisof gastric origin: a population-based study on incidence, survivaland risk factors. Int J Cancer 2014; 134: 622–8.

3 Park DI, Yun JW, Park JH et al. HER-2/neu amplification is an independentprognostic factor in gastric cancer. Dig Dis Sci 2006; 51: 1371–9.

4 Bang YJ, Van Cutsem E, Feyereislova A et al. Trastuzumab in combinationwith chemotherapy versus chemotherapy alone for treatment of HER2-positiveadvanced gastric or gastro-oesophageal junction cancer (ToGA): a phase

5 3, open-label, randomised controlled trial. Lancet 2010; 376: 687–97.

6 Pouget JP, Navarro-Teulon I, Bardies M et al. Clinical radioimmunotherapy–the role of radiobiology. Nat Rev Clin Oncol 2011; 8: 720–34.

7 Larson SM, Carrasquillo JA, Cheung NK, Press OW. Radioimmunotherapyof human tumours. Nat Rev Cancer 2015; 15: 347–60.

8 Janik JE, Morris JC, O'Mahony D et al. 90Y-daclizumab, an anti-CD25 monoclonal antibody, provided responses in 50% of patients with relapsed Hodgkin's lymphoma. Proc Natl Acad Sci USA 2015; 112: 13045–50.

9 Li HK, Morokoshi Y, Daino K et al. Transcriptomic signatures of auger electron radioimmunotherapy using nuclear targeting (111)in-trastuzumab for potential combination therapies. Cancer Biother Radiopharm 2015; 30: 349–58.

10 Couturier O, Supiot S, Degraef-Mougin M et al. Cancer radioimmunotherapywith alpha-emitting nuclides. Eur J Nucl Med Mol

Imaging 2005; 32: 601–14.
11 Zalutsky MR, Pruszynski M. Astatine-211: production and availability. CurrRadiopharm 2011; 4: 177–85.
12 Nikula TK, McDevitt MR, Finn RD et al. Alpha-emitting bismuth cyclohexylbenzyl DTPA constructs of recombinant humanized anti-CD33 antibodies: pharmacokinetics, bioactivity, toxicity and chemistry. J Nucl Med 1999;40: 166–76.
13 McDevitt MR, Ma D, Lai LT et al. Tumor therapy with targeted atomic nanogenerators. Science 2001; 294: 1537–40.
14 Nagatsu K, Minegishi K, Fukada M, Suzuki H, Hasegawa S, Zhang MR. Production of (211)At by a vertical beam irradiation method. Appl Radiat Isot 2014; 94: 363–71.
15 Lindegren S, Frost S, Back T, Haglund E, Elgqvist J, Jensen H. Direct procedure for the production of 211At-labeled antibodies with an epsilon-lysyl-3-(trimethylstannyl)benzamide immunoconjugate. J Nucl Med 2008; 49:1537–45.
16 Chrestensen CA, Shuman JK, Eschenroeder A, Worthington M, Gram H, Sturgill TW. MNK1 and MNK2 regulation in HER2-overexpressing breast cancer lines. J Biol Chem 2007; 282: 4243–52.
17 Cederkrantz E, Angenete E, Back T et al. Evaluation of effects on the peritoneum after intraperitoneal alpha-radioimmunotherapy with (211)At. Cancer Biother Radiopharm 2012; 27: 353–64.
18 Frost SH, Back T, Chouin N et al. Comparison of 211At-PRIT and 211At-RIT of ovarian microtumors in a nude mouse model. Cancer Biother Radiopharm 2013; 28: 108–14.
19 Derrien A, Gouard S, Maurel C et al. Therapeutic efficacy of alpha-rit using a (213)Bi-Anti-hCD138 antibody in a mouse model of ovarian peritoneal carcinomatosis. Front Med (Lausanne) 2015; 2: 88.
20 Andersson H, Cederkrantz E, Back T et al. Intraperitoneal alpha-particle radioimmunotherapy of ovarian cancer patients: pharmacokinetics and dosimetry of (211)At-MX35 F(ab')2–a phase I study. J Nucl Med 2009; 50:1153–60.

21 Palm S, Back T, Claesson I et al. Therapeutic efficacy of astatine-211-labeled trastuzumab on radioresistant SKOV-3 tumors in nude mice. Int J Radiat Oncol Biol Phys 2007; 69: 572–9.
22 Lewis Phillips GD, Li G, Dugger DL et al. Targeting HER2-positive breast cancer with trastuzumab-DM1, an antibody-cytotoxic drug conjugate. Cancer Res 2008; 68: 9280–90.
23 Verma S, Miles D, Gianni L et al. Trastuzumab emtansine for HER2-positive advanced breast cancer. N Engl J Med 2012; 367: 1783–91.

**Cancer Science 108(8):1648-1656**

平成 **29** 年 **6** 月 **27** 日　公開済み